

NLTE study of scandium in the Sun

H.W. Zhang^{1,2}, T. Gehren², and G. Zhao³

¹ Department of Astronomy, School of Physics, Peking University, Beijing 100871, P.R. China

² Institut für Astronomie und Astrophysik der Universität München, Scheinerstrasse 1, D-81679 München, Germany

³ National Astronomical Observatories, Chinese Academy of Sciences, Beijing 100012, P.R. China

Received ; accepted

ABSTRACT

Aims. We investigate the formation of neutral and singly ionized scandium lines in the solar photospheres. The research is aimed derive solar $\log gf\varepsilon_{\odot}(\text{Sc})$ values for scandium lines, which will later be used in differential abundance analyses of metal-poor stars.

Methods. Extensive statistical equilibrium calculations were carried out for a model atom, which comprises 92 terms for Sc I and 79 for Sc II. Photoionization cross-sections are assumed to be hydrogenic. Synthetic line profiles calculated from the level populations according to the NLTE departure coefficients were compared with the observed solar spectral atlas. Hyperfine structure (HFS) broadening is taken into account.

Results. The statistical equilibrium of scandium is dominated by a strong underpopulation of Sc I caused by missing strong lines. It is nearly unaffected by the variation in interaction parameters and only marginally sensitive to the choice of the solar atmospheric model. Abundance determinations using the ODF model lead to a solar Sc abundance of between $\log \varepsilon_{\odot} = 3.07$ and 3.13, depending on the choice of f values. The long known difference between photospheric and meteoritic scandium abundances is confirmed for the experimental f -values.

Key words. line: formation - line: profiles - sun: abundances

1. Introduction

According to the theory of nucleosynthesis, the α elements are mostly produced by Type II supernovae, while some iron-peak elements have significant contributions from Type Ia supernovae. The synthesis process and sites of scandium, as an element intermediate between α elements and iron-peak elements in the periodic table, are not clear now.

The variation of the scandium abundance pattern in long-lived F- and G-type stars with different metallicity can provide some information on the element nucleosynthesis and the chemical evolution of the Galaxy. There is an unresolved inconsistency between different Sc abundance results. In some analyses, an Sc *enhancement* relative to Fe is found in metal-poor stars (e.g. Zhao & Magain 1990, Nissen et al. 2000); however, others (e.g. Gratton & Sneden 1991, Prochaska & McWilliam 2000) found no evidence of any deviation from $[\text{Sc}/\text{Fe}] = 0.0$.

Generally, the solar photospheric abundances serve as a reference for abundance determinations in metal-poor stars, so a reliable set of photospheric abundances is important. Ever since Anders & Grevesse (1989) published their widely used solar elemental abundance table, many revisions and updates to photospheric and meteoritic abundances of the elements have become available, although the solar *photospheric* scandium abundance has not been updated for quite a long time. The photospheric abundance value of $\log \varepsilon_{\odot}(\text{Sc}) = 3.10 \pm 0.09$ adopted by Grevesse (1984) was changed to 3.05 ± 0.08 by Youssef & Amer (1989). Neuforge (1993) obtained 3.14 ± 0.12 from the Sc I lines and 3.20 ± 0.07 from Sc II lines. The average value of 3.17 ± 0.10 was adopted by Grevesse & Noels (1993) and was kept in the

newest tabular version of Grevesse et al. (2007), which is somewhat higher than the meteoritic value of 3.04 ± 0.04 .

It should be noted that local thermodynamic equilibrium (LTE) has been assumed in previous papers about scandium abundance determinations, and NLTE investigation of the scandium element has never been published. In general, departures from LTE are commonplace and often quite important, in particular for low surface gravities or metallicities, with minority ions and low-excitation transitions the most vulnerable (see the review paper of Asplund 2005). In the Sun and other near-turnoff stars, the ionization energy of Sc I (6.56 eV, see Fig. 1) indicates that this is a *minority ion*. Lines of Sc I should therefore be more susceptible to NLTE, because any small change in the ionization rates largely changes the populations of the minor ion, although there is no guarantee that Sc II lines behave properly in a standard LTE analysis.

In this paper we investigate the statistical equilibrium and formation of neutral and singly-ionized scandium lines in the solar photosphere. We note that we do not intend to study the influence of atmospheric inhomogeneities on any scale or that of chromospheric temperatures and pressures. The method of NLTE calculations is briefly introduced in Sect. 2. In Sect. 3 the synthesis of the Sc I and Sc II lines under NLTE and hyperfine structure is presented. The discussion fills the last section.

2. NLTE line formation calculations

Abandoning the LTE approximation introduces a great deal of additional complexity into the line formation calculations. Under NLTE conditions, the atomic populations are described by a set of statistical equilibrium equations in which radiative and collisional processes are to be taken into account. Our calculations

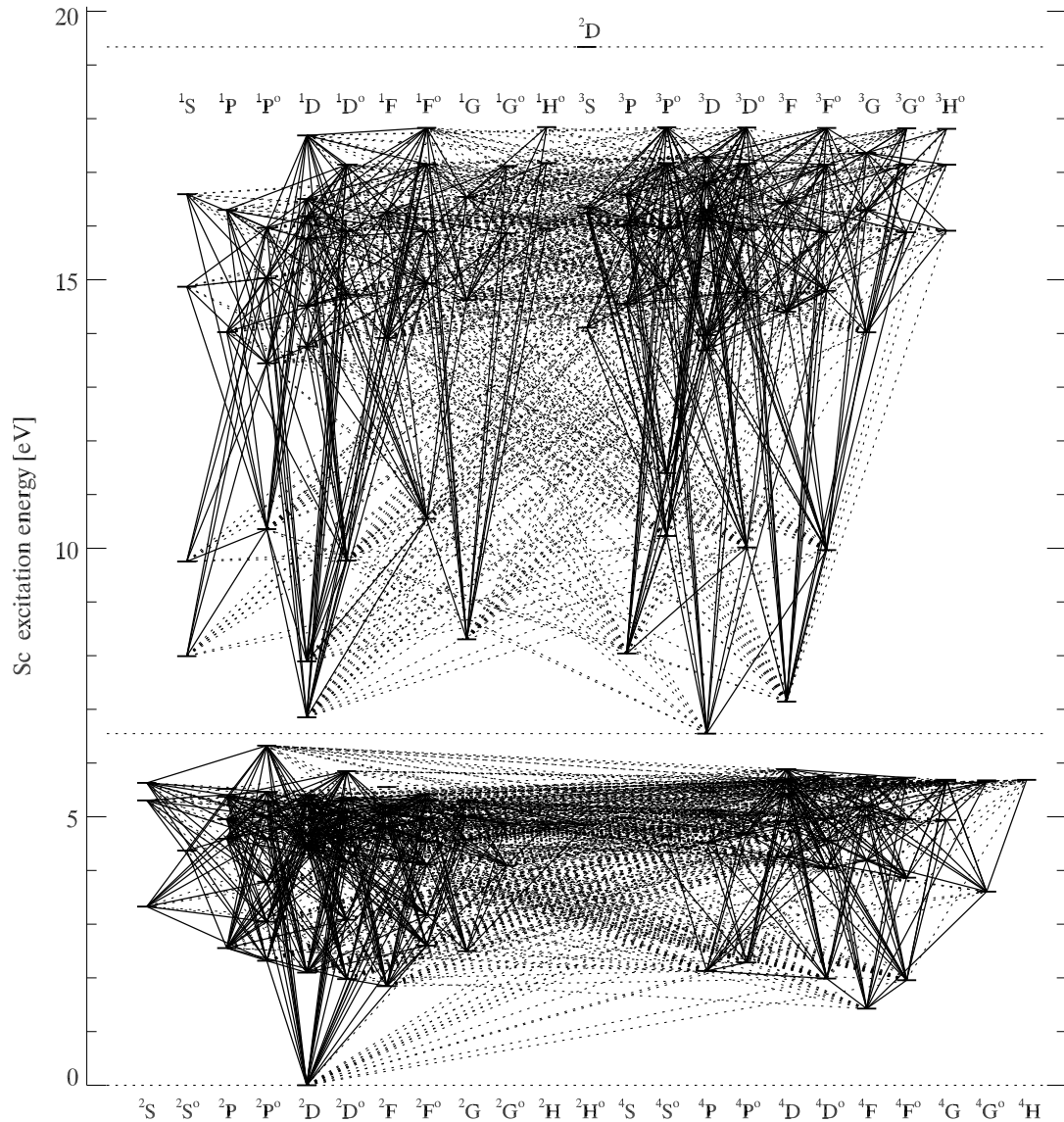


Fig. 1. Adopted level structure of the Sc I and Sc II atom taken from the NIST data bank. Explicitly calculated line transitions are indicated, where continuous lines refer to allowed and dotted lines to forbidden transitions according to selection rules assuming LS coupling.

were carried out with a revised version of the DETAIL program (Butler & Giddings 1985), which solves the radiative transfer and statistical equilibrium equations by the method of accelerated lambda iteration.

Our calculations were performed on a partially ionized background medium consisting of a plane-parallel, homogeneous, line-blanketed theoretical model of the solar photosphere, which includes a simple approach to convective equilibrium based on the mixing-length theory. The model was computed with the MAFAGS code (Fuhrmann et al. 1997). In contrast to the line formation itself, the *atmospheric* model assumes LTE to obtain the final temperature-pressure stratification. It uses opacity distribution functions (ODF) for line-blanketing, based on Kurucz (1992), and calculated with opacities rescaled to a solar iron abundance $\log \varepsilon_{\odot}(\text{Fe}) = 7.51$ (more details are found in Gehren et al. 2001). The resulting atmospheric stratifications of tempera-

ture and pressure are similar to those given by other solar models (see comparison in Grupp 2004, Fig. 15).

2.1. Atomic model

A comprehensive atomic model is required for NLTE calculations. Similar to other iron-group elements, scandium has a complex atomic structure. Our atomic reference model is constructed from 256 and 148 *levels* for neutral and singly-ionized scandium, respectively. Energies for these levels are taken from the NIST data bank¹. After a few early test calculations with this complete fine structure model, we found that the calculations could be considerably reduced by combining all fine structure levels into 92 and 79 *terms* for Sc I and Sc II, respectively. The corresponding fine structure data were appropriately weighted

¹ <http://www.physics.nist.gov/>

to determine term energies. The atomic term model used for our calculations is displayed in Fig. 1. It shows that completeness is fading at high excitation energies, with energy gaps of between 0.3 and 1.0 eV for the neutral doublets and quartets, and gaps of ~ 1.5 eV for the ionized singlets and triplets.

The number of bound-bound *transitions* treated in the NLTE calculations is 1104 for Sc I and 1034 for Sc II, numbers again considerably reduced from the original *level* transitions. Wavelengths and oscillator strengths of the fine structure transitions are taken from Kurucz's database (Kurucz & Bell 1995), and they are weighted by statistical weights to yield artificial term transitions. A Grotrian diagram for Sc I and Sc II is displayed in Fig. 1. Solid and dotted lines represent the allowed and forbidden transitions included in the model atom, respectively. Since the reduction of the fine structure model atom does not affect the resulting calculations of the population densities, it is unlikely that the hyperfine structure (HFS) has any direct influence on the NLTE results, particularly since the known HFS is small.

For bound-free radiative transitions in the Sc atom, hydrogen-like photoionization cross-sections (Mihalas 1978) are adopted, because data from the Opacity Project (OP; see Seaton et al. 1994) are not available. In our current analysis this may be the most uncertain representation. In previous studies of Fe (Gehren et al. 2001), and K (Zhang et al. 2006), where complex calculations of such cross-sections were available, we found that hydrogenic approximations occasionally tend to underestimate the photoionization cross-sections by one or two orders of magnitude. The effect on the NLTE analysis is examined below.

As usual, *background opacities* are calculated with an opacity sampling code based on the line lists made available by Kurucz (1992). Since background opacities affect the photoionization rates directly, their consideration is important. We note, however, that the millions of faint lines, which may be somewhat more important for model atmosphere construction, are marginal for our line formation calculations.

In our calculations for Sc, we take into account inelastic collisions with electrons and hydrogen atoms leading to both excitation and ionization. Because laboratory measurements and detailed quantum mechanical calculations for collision cross-sections are absent, approximate formulae are applied. The formulae of van Regemorter (1962) and Allen (1973) are used to describe the excitation of allowed and forbidden transitions by electron collisions, respectively. Ionization cross-sections for electron collisions are calculated with the formula of Seaton (1962). Drawin's (1968, 1969) formula as described by Steenbock & Holweger (1984) is used to calculate neutral hydrogen collisions. Recently it was indicated both experimentally and theoretically that Drawin's formula overestimates the H collisional cross-section by one to six orders of magnitude (e.g. Belyaev et al. 1999, Belyaev & Barklem 2003), so a scaling factor S_H is applied to the Drawin formula in our calculations, for which results are given below.

2.2. NLTE level populations

The atomic model described above still has a number of free parameters that represent our ignorance of the microscopic interaction processes. Whereas the number of levels (terms) and lines (transitions) comprises the basic structure of the two lower scandium ions, it is the interactions that require some additional fine tuning. As explained above, we introduce standard multiplication factors for electron collisions, hydrogen collisions, and photoionization cross-sections. These factors are defined with

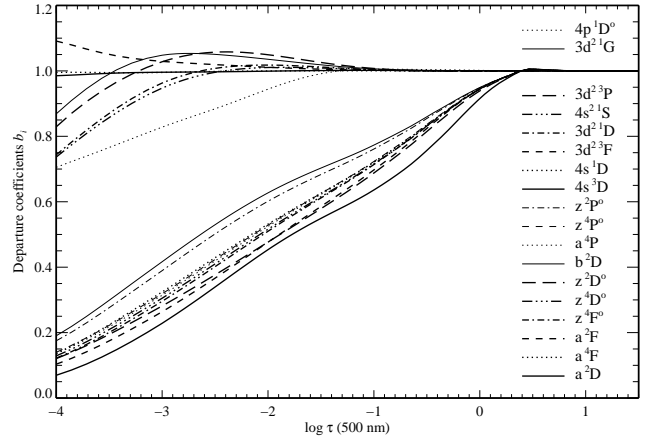


Fig. 2. Departure coefficients b_n for some levels of Sc I and Sc II in the ODF solar atmospheric model applying our standard atomic model with multiplication factors $S_e = 1$, $S_H = 0.1$, and $S_p = 1$ for bound-bound electron collisions, bound-bound hydrogen collisions, and bound-free photoionization coefficients, respectively. The kinetic equilibrium calculations are described in the text.

respect to the standard formulae for these three types of processes, which were mentioned in section 2.1. Using the *standard atomic model*, departure coefficients $b_k = n_k^{\text{NLTE}}/n_k^{\text{LTE}}$ for Sc I and Sc II terms in the solar atmosphere are presented in Fig. 2. The standard model refers to $S_e = 1$, $S_H = 0.1$, and $S_p = 1$.

Since there are no other strong indicators, it is necessary to explore the influence of such a parametric variation in interaction strengths on the level population densities. This is done by varying only one parameter at a time while holding all others at their standard values, and the results are surprising in that we find no strong influence for either of the multiplication factors (Fig. 3). All calculations represented here document the extreme weakness of the solar Sc I lines resulting from both the low abundance and the low ionization potential. All lines thus form in the same atmospheric depths as the local H^- continuum. There the mean integrated line intensities become constant (and the *net* bound-bound radiative rates positive, or upwards) outside $\tau \simeq 1$. All the *lower levels* (those with less than 3...4 eV excitation energy) are therefore depopulated by this collective pumping process, whereas the upper levels are simultaneously populated. However, no true population inversion is achieved. Photoionization rates from the lower levels are low, but mostly higher than the corresponding recombination rates. This again supports the depopulation of the lower levels throughout the solar atmosphere. Of course, the radiative rates are modified by collision rates, and the total rates are driven more towards zero net rates, but this does not prevent the general depopulation trend.

Figure 3 demonstrates clearly that even relatively large variations in the multiplication factors do not change the run of the level populations too much. There are thermalizing effects when increasing electron or hydrogen collision factors, but these affect the population *ratios*, and not the departure coefficients themselves very much. A notable exception is represented by the $S_e = 10$, because this starts to couple the lower terms more efficiently to the upper ones and thus thermalizes the whole Sc I system. The lack of variation with S_p is simply due to the decoupling of

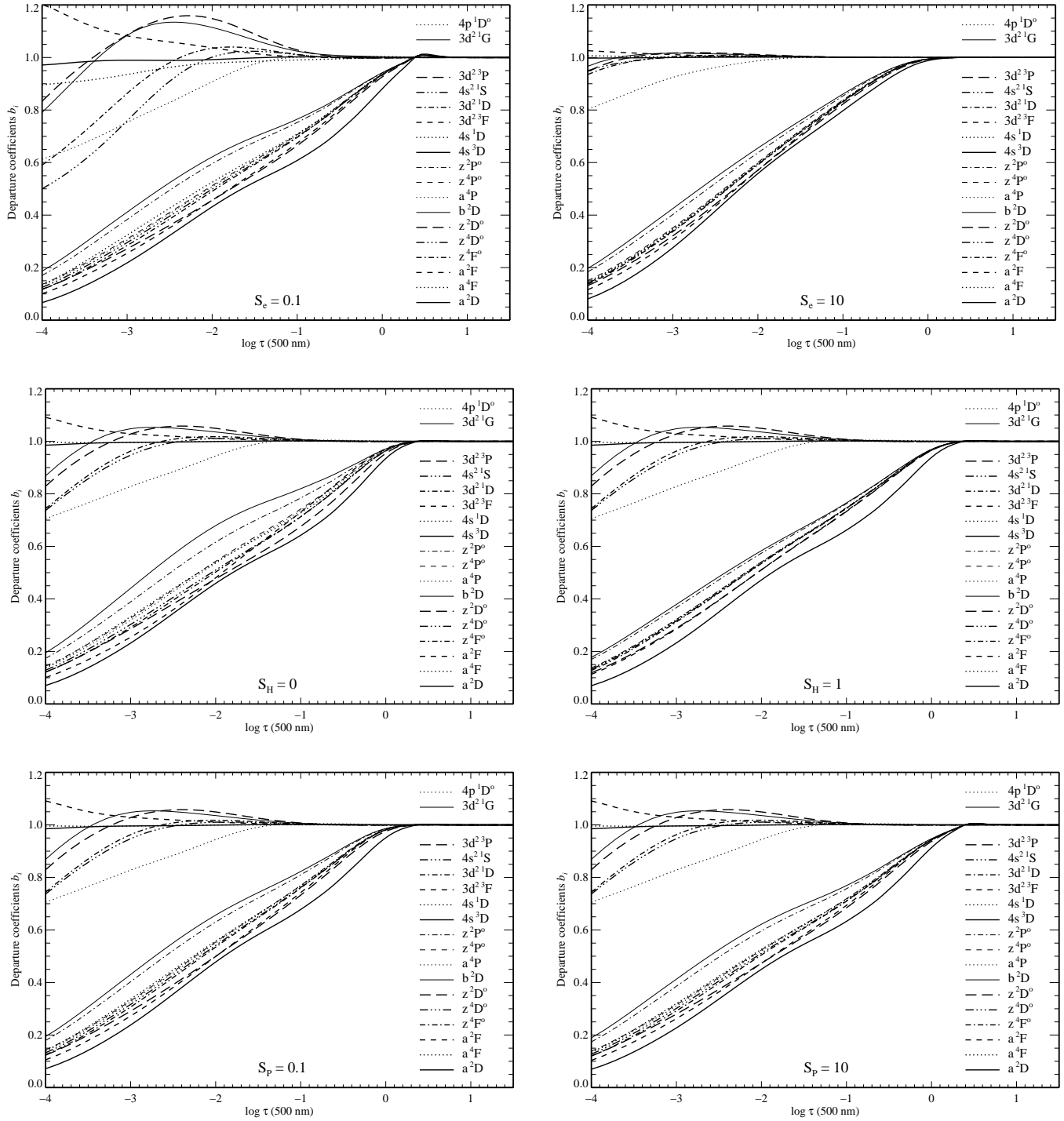


Fig. 3. Departure coefficients b_n for levels of Sc I and Sc II in the ODF solar atmospheric model testing the multiplication factors $S_c = 0.1$ and 10 (top), $S_H = 0$ and 1 (middle), and $S_p = 0.1$ and 10 (bottom).

the radiation field and the small hydrogen-like photoionization cross-sections.

Sc II is the dominant ion of the element under solar atmospheric conditions, with more than 99% of the scandium atoms being ionized under the atmospheric conditions found in the Sun. Its lines are substantially stronger than those of Sc I, although not comparable in line strength with other metals. Only the strongest lines form outside $\log \tau \approx -1$. Figure 3 shows that all Sc II lines

in the visible spectrum are formed near to LTE conditions. There is no clear indication how to select the proper scaling factors. In view of the minor changes due to parameter variation, we choose typical factors to establish the standard model atom (see Fig. 2). Since this choice may affect the line formation in stars different from the Sun, we will extend the analysis for metal-poor stars to obtain a more significant choice of the scaling factors.

Table 1. Atomic data and abundance results for Sc I and Sc II lines.

λ [Å]	Mult	Lower level	Upper level	E_{low} [eV]	W_{λ} [mÅ]	$\log gf$ Kurucz	$\log gf$ LD	$\log C_6$	$\log \varepsilon$ ODF	$\log \varepsilon$ OS	Δb	ΔX	$\log gf \varepsilon_{\odot}$ NLTE	HFS N	HFS $\Delta \lambda$	–
Sc I																
4023.690	5	$a^2D_{5/2}$	$y^2D_{5/2}^o$	0.02	51.9	0.405	0.381	-31.780	3.04	3.05	0.00	+0.27	3.44	16	12	*
5081.550	7	$a^4F_{9/2}$	$y^4F_{9/2}^o$	1.44	11.7	0.492	0.469	-31.873	3.12	3.15	-0.04	+0.16	3.61	22	86	*
5671.800	6	$a^4F_{9/2}$	$z^4G_{11/2}^o$	1.44	14.4	0.534	0.495	-31.955	3.12	3.15	-0.04	+0.15	3.66	21	95	
5686.830	6	$a^4F_{7/2}$	$z^4G_{9/2}^o$	1.43	9.1	0.415	0.376	-31.955	3.03	3.06	-0.07	+0.14	3.45	21	56	
Sc II																
4246.830	1	$4s^1D_2$	$4p^1D_2^o$	0.32	160.6	0.283	0.241	-32.088	3.05	3.09	0.00	-0.04	3.33	13	21	*
4314.087	5	$3d^2^3F_4$	$4p^3D_3^o$	0.62	116.9	-0.050	-0.097	-32.040	3.06	3.08	-0.07	-0.03	3.01	20	11	
4320.743	5	$3d^2^3F_3$	$4p^3D_2^o$	0.60	108.2	-0.212	-0.252	-32.040	3.05	3.08	-0.03	-0.06	2.84	15	9	
4400.350	4	$3d^2^3F_3$	$4p^3F_3^o$	0.60	96.3	-0.513	-0.537	-32.118	3.11	3.16	-0.04	-0.06	2.60	18	20	
4670.400	12	$3d^2^1D_2$	$4p^1F_3^o$	1.35	63.5	-0.518	-0.576	-31.996	3.03	3.04	-0.04	-0.04	2.51	15	17	
5031.020	11	$3d^2^1D_2$	$z^1P_1^o$	1.35	75.4	-0.341	-0.400	-32.081	3.06	3.06	-0.03	-0.03	2.72	9	20	*
5357.200	19	$3d^2^3P_2$	$z^1P_1^o$	1.50	4.3	-2.143	-2.111	-32.068	3.16	3.17	-0.01	0.00	1.02	9	4	*
5526.810	21	$3d^2^1G_4$	$4p^1F_3^o$	1.76	77.4	0.064	0.024	-31.995	3.08	3.08	0.00	-0.08	3.14	20	25	
5640.970	18	$3d^2^3P_1$	$z^3P_2^o$	1.49	37.6	-0.990	-1.131	-32.151	3.05	3.06	-0.02	-0.02	2.06	9	27	
5657.870	18	$3d^2^3P_2$	$z^3P_2^o$	1.50	63.3	-0.491	-0.603	-32.151	3.09	3.10	0.00	-0.08	2.62	13	23	
5667.160	18	$3d^2^3P_1$	$z^3P_0^o$	1.49	29.3	-1.191	-1.309	-32.151	3.11	3.12	0.00	-0.01	1.92	7	31	
5669.030	18	$3d^2^3P_1$	$z^3P_0^o$	1.49	33.7	-1.072	-1.200	-32.151	3.09	3.09	0.00	-0.01	2.02	1	0	*
5684.190	18	$3d^2^3P_2$	$z^3P_0^o$	1.50	36.0	-0.998	-1.074	-32.151	3.09	3.09	0.00	-0.02	2.09	9	27	
6245.630	17	$3d^2^3P_2$	$4p^3D_3^o$	1.50	35.7	-1.030		-32.057	3.02	3.03	0.00	-0.02	1.99	15	37	
6279.760	17	$3d^2^3P_1$	$4p^3D_2^o$	1.49	28.8	-1.265		-32.057	3.14	3.15	-0.02	-0.02	1.88	9	38	
6300.685	17	$3d^2^3P_2$	$4p^3D_2^o$	1.51	7.3	-1.887		-32.057	2.98	3.00	-0.04	-0.01	1.09	13	33	
6320.867	17	$3d^2^3P_1$	$4p^3D_1^o$	1.50	8.8	-1.819		-32.057	3.07	3.08	0.00	0.00	1.25	7	44	

3. Analysis of scandium lines in the solar spectrum

In this section, we investigate the formation of Sc I and Sc II lines in the solar atmosphere and derive the scandium abundance based on spectrum synthesis. Lines in the solar spectrum are calculated using the plane-parallel hydrostatic MAFAGS-ODF solar model atmosphere with $T_{\text{eff}} = 5780$ K, $\log g = 4.44$, $[\text{Fe}/\text{H}] = 0.00$, $\xi_t = 0.90$ km s $^{-1}$ (for a more detailed comparison with *opacity sampling* models see Grupp 2004). An initial scandium abundance of $\log \varepsilon_{\odot}(\text{Sc}) = 2.99$ is adopted here. It should be noted that the atmospheric model of the Sun does *not* depend on the scandium abundance. For all elements except scandium, we assume LTE.

3.1. Atomic line data

For the solar abundance analysis we selected 4 Sc I and 17 Sc II lines, which ideally should satisfy the following conditions: they are relatively free from blends, and oscillator strengths and hyperfine splitting parameters are available. However, both conditions are not always guaranteed. In particular, HFS data for the ground state of Sc II are missing making the analysis of the corresponding lines more uncertain. Unfortunately, the number of sufficiently strong lines in the visible of both ions is very limited, and in metal-poor stars this requires concentration on the leading lines of Sc II, since the equivalent width of Sc I 4023 in typical turnoff stars is less than 0.5 mÅ.

To determine the solar abundance, it is necessary to know the accurate oscillator strengths (f values) of the spectral lines. Two sets of oscillator strengths are applied and compared in our abundance determinations: (i) theoretical values taken from Kurucz' database², and (ii) experimental data of Lawler & Dakin

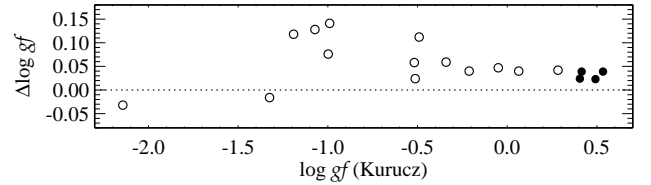


Fig. 4. Comparison of $\log gf$ -values from different sources. Filled circles represent the Sc I ion, open circles refer to Sc II. $\Delta \log gf$ means Kurucz – Lawler & Dakin.

(1989), which were based on lifetimes measured by Marsden et al. (1988) together with branching fractions. Van der Waals damping constants $\log C_6$ are computed according to the Anstee & O'Mara (1991, 1995) interpolation tables. Input parameters needed to perform spectrum synthesis for the selected lines are given in Table 1. The different sets of f -values from Kurucz and from Lawler & Dakin are compared in Fig. 4. There is a small systematic offset between the two data sets, with a mean $\Delta \log gf(\text{Kur} - \text{LD}) \approx 0.05$. The corresponding line data for our line fits are reproduced in Table 1.

In solar system matter, scandium is represented only by the ^{45}Sc isotope. Similar to other odd-Z elements, hyperfine structure interactions between nuclear and electronic wave functions split the absorption lines of Sc into multiple components. Hyperfine structure components of line transitions are calculated as usual from magnetic dipole splitting constants, $A(J)$, and electric quadrupole splitting constants, $B(J)$, of the corresponding levels. For most of the lines the HFS components fall into small intervals; we therefore combine all components within 5 mÅ (Sc I) or 10 mÅ (Sc II), which reduces many HFS patterns

² <http://kurucz.harvard.edu>, see also Kurucz & Bell (1995)

Table 2. Hyperfine structure data for Sc I and Sc II levels used in this analysis.

Level	E [eV]	$A(J)^*$	$B(J)^*$	Reference
Sc I				
$a^2D_{5/2}$	0.0209	0.00363	-0.00124	Childs (1971)
$a^4F_{7/2}$	1.4395	0.0083	-0.0003	Ertmer & Hofer (1976)
$a^4F_{9/2}$	1.4478	0.0095	-0.0004	Ertmer & Hofer (1976)
$z^4G_{9/2}^o$	3.6191	0.0029		Ertmer & Hofer (1976)
$z^4G_{11/2}^o$	3.6332	0.0015		Ertmer & Hofer (1976)
Sc II				
$3d^2\ ^3F_3$	0.6054	0.00379	-0.00042	Mansour et al. (1989)
$3d^2\ ^3F_4$	0.6184	0.00128	-0.00055	Mansour et al. (1989)
$3d^2\ ^1D_2$	1.3570	0.00498	0.00026	Mansour et al. (1989)
$3d^2\ ^3P_1$	1.5004	-0.00359	-0.00041	Mansour et al. (1989)
$3d^2\ ^3P_2$	1.5070	-0.00093	0.00074	Mansour et al. (1989)
$3d^2\ ^1G_4$	1.7682	0.00451	-0.00212	Mansour et al. (1989)
$4p\ ^1D_2^o$	3.2337	0.00719	0.00060	Arnesen et al. (1982)
$4p\ ^3F_3^o$	3.4223	0.00685	-0.00233	Young et al. (1988)
$4p\ ^3D_2^o$	3.4742	0.00418	0.00033	Mansour et al. (1989)
$4p\ ^3D_3^o$	3.4915	0.00332	0.00070	Mansour et al. (1989)
$4p\ ^1F_3^o$	4.0109	0.00637	-0.00274	Mansour et al. (1989)
$z^3P_0^o$	3.6876	0.00851	0.00033	Mansour et al. (1989)
$z^3P_2^o$	3.6977	0.00354	0.00067	Mansour et al. (1989)
$4p\ ^3D_1^o$	3.4614	0.01016	0.00015	Mansour et al. (1989)
$4p\ ^3D_2^o$	3.4742	0.00418	0.00033	Mansour et al. (1989)
$4p\ ^3D_3^o$	3.4915	0.00332	0.00070	Mansour et al. (1989)

*: in units of cm^{-1} .

to two or three coadded lines. The basic data are given in Table 2. Abundance differences with respect to the full HFS pattern are all within 0.01 dex.

3.2. Line profile fitting

The observed solar flux spectrum was taken from the Kitt Peak Atlas (Kurucz et al. 1984). Spectrum synthesis was employed to determine the abundance of scandium in the solar atmosphere. As in earlier work we used the interactive spectral line-profile fitting program SIU, which is an IDL/Fortran software package (Reetz 1990). To match the observed spectral lines, the synthetic spectra were convolved with a mean solar rotational velocity of 1.8 km s^{-1} and a radial-tangential macroturbulence Ξ_r which is found to vary for lines of different mean depth of formation between 2.8 and 4.0 km s^{-1} .

Except for the obvious influence of strong metal or Balmer line wings in the spectral range under consideration, we reset the local continuum position interactively to the maximum flux in a $\pm 5\text{ \AA}$ interval around the line center. This is never a problem, because our spectrum synthesis includes all important lines and thus allows confirmation of the local maximum flux estimate. Any uncertainty in this process, even in the yellow wavelength range between 5700 and 5850 \AA where the solar atlas displays a continuum that is systematically high by $\sim 2\%$, is smaller than the general profile fitting error. Our estimate of its influence on the abundances is ~ 0.01 dex.

Line profiles are computed under both LTE and NLTE assumptions: fitted to the observed profiles by means of scandium abundance variations. Column 10 of Table 1 reproduces the log-

arithmic abundances $\log \varepsilon$ of the fits including a number of weak blends on either side of the profiles. They are based on Kurucz' $\log gf$ values and NLTE level populations. The logarithmic corrections due to weak blends are listed in the Δb column. Thus, fitting the lines *without* blends would have resulted in a *higher* logarithmic abundance $\log \varepsilon - \Delta b$. The difference required to fit LTE and NLTE profiles is referred to as the *NLTE correction* ($\Delta X = \log \varepsilon^{\text{NLTE}} - \log \varepsilon^{\text{LTE}}$); it is given in column 13 of Table 1 for each line. Equivalent widths from NLTE profile fits (see Fig. 5) are given in column 6 of Table 1. The last three columns give the number of components, the maximum wavelength separation (in m\AA) of the hyperfine structure (HFS) lines and an asterisk, if HFS data are missing for one of the levels(cf. Table 2).

Some of the synthetic profiles for selected lines, together with the observed solar spectrum, are presented in Fig. 5. Whenever available, we have included known blends. For comparison we show profiles under LTE and NLTE conditions including HFS. Generally, all neutral lines are much fainter in NLTE due to significant underpopulation, whereas lines of ionized scandium are slightly stronger under NLTE conditions.

A marginal *line core asymmetry* with the observed line bisectors shifted 1 or 2 m\AA to the red seems to exist. This is known from the solar spectrum synthesis of other metals, such as Si, Ca, or Mn. It is probably the result of hydrodynamic streaming patterns that cannot be represented by our simple micro/macroturbulence scheme. A more disturbing defect is the near-continuum flux deficiency of the red line wing, best seen in the 5657 and 6245 \AA lines. This feature is also found in other metals. Sometimes addressed as the result of a weak line haze or blends, the systematic blue-red asymmetry is more likely to result from hydrodynamic flows, too. We emphasize, however, that this wavelength region displays a particularly disturbed solar continuum flux. Table 1 already gives a hint that some of the lines synthesized here suffer from missing HFS data. Unfortunately, the strongest lines of both ions are affected, requiring more detailed comments.

Sc I 4023.69 \AA has been calculated with only the HFS split of the $a^2D_{5/2}$ level. That this is possibly a fair but not perfect representation of the true hyperfine structure width of the line is documented in Fig. 5a, where the synthesized line halfwidth fits that of the solar spectrum. However, the total separation of the HFS components is small (see Table 1). Another distortion is caused by a number of faint line blends on the red core and wing of this line. The known components are two highly excited faint Mn I lines at 4023.72 and 4023.84 \AA , for which no HFS data are available. There is also a faint Cr I line at 4023.74 \AA . These blends have been considered in Fig. 5a, but even the two lines within 50 m\AA of the Sc I line center have no influence on the fit of the core. Introducing these blend components and fitting the full core profile results in a Sc line abundance change below 0.01 dex. The remaining red wing depression centered on 4023.84 \AA may be the result of the unknown Mn I HFS.

Sc I 5081.55 , 5671.80 , and 5686.83 \AA are substantially fainter neutral Sc lines, with solar equivalent widths of only 12, 14, and 9 m\AA , respectively. That makes the line abundances be sensitive to the continuum position, which is particularly uncertain between 5600 and 5700 \AA . Only one of the lines is presented in Fig. 5b. Although most of the Sc lines were chosen to be as free of blends as possible, the wings of the 5671.80 \AA line are covered by quite a few weak lines of Mn I, Fe I, and Ti I, all of which are in the range of equivalent widths between 0.5 and 1.5 m\AA . These lines have central depths between 1 and 2% of the

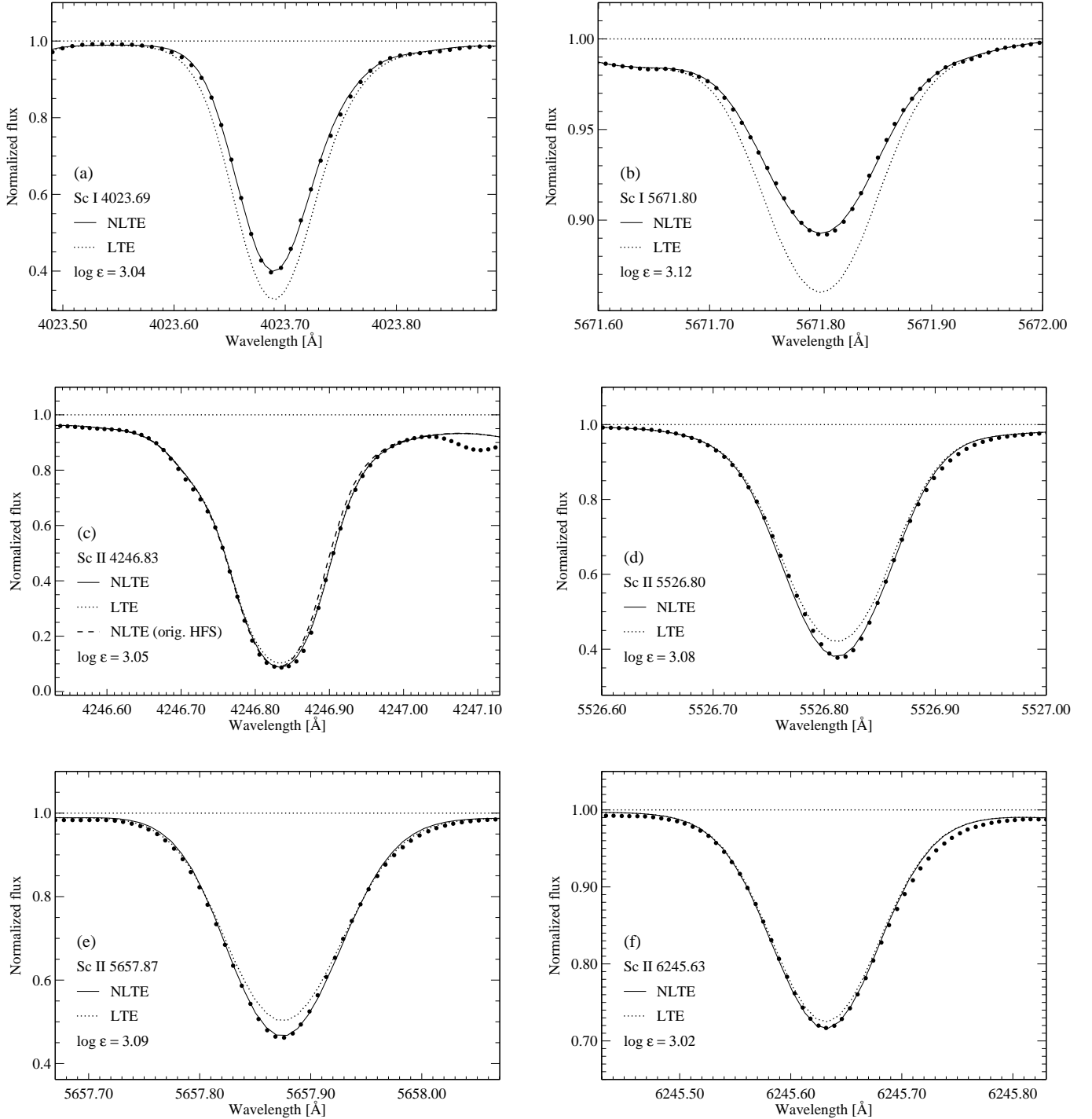


Fig. 5. Representative solar line profiles for Sc I and Sc II. Always shown are the NLTE and LTE profiles for the given abundance, where the NLTE profiles refer to the best fit. λ 4246.83 additionally shows the NLTE line with the *originally calculated* HFS components (second component at 4246.839 instead of 4246.844 Å, see text).

continuum flux, and their (gaussian) wings give some combined contribution to the Sc line core. Thus the full influence of the weak blends on the Sc abundance of this line is -0.04 dex. For the other two lines, the blend corrections are -0.04 and -0.07 , respectively.

Sc II 4246.83 Å is one of the strongest lines of Sc II in the visible. It contains two weak blends on the blue line wing. Due to missing HFS data for the lower level, a^1D_2 , the resulting profiles

are not as reliable as those obtained for the excited levels. This is evident from Fig. 5c, where the line width of the profile with the originally calculated HFS components does not fit the observed solar profile unless the HFS separation is increased by 5 mÅ moving the second component from 4246.839 Å to 4246.844 Å. This is a purely empirical correction; however, it is the only way to fit the solar line profile without postulating an unknown blend.

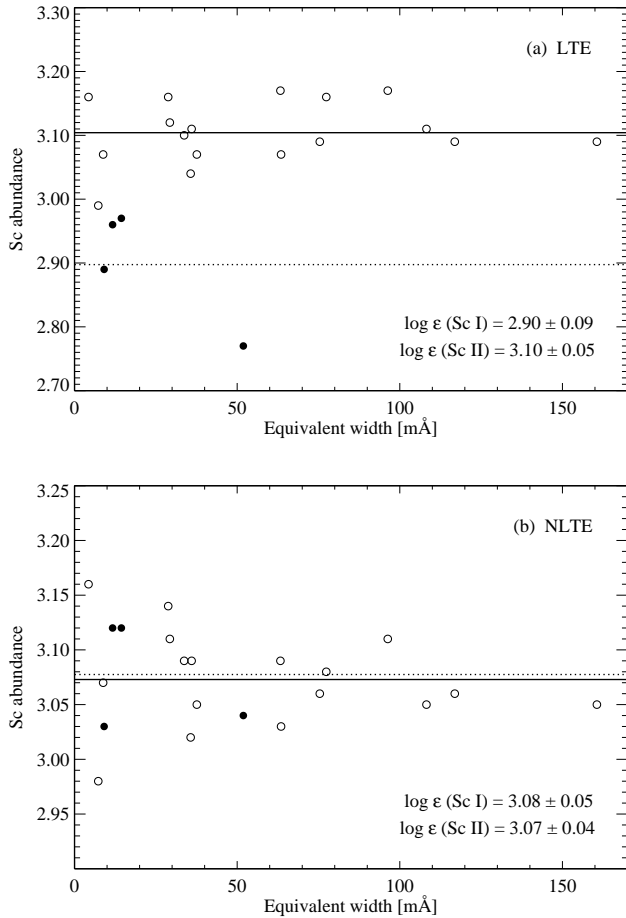


Fig. 6. Solar Sc abundances based on Kurucz gf values for lines of Sc I (filled circles) and Sc II (open circles) plotted as function of the line equivalent widths. The mean abundance from Sc I lines is represented by the dotted line, that of Sc II by a continuous line. Top: LTE, bottom: NLTE.

Sc II 5526.81 Å and 5657.87 Å (Figs. 5d and e) represent the lines on the flat part of the curve-of-growth; i.e., they strongly depend on the microturbulence parameter. Their hyperfine structure is known and seems to fit the solar spectrum for both lines. There are two blends on the red wing of the 5526 Å line, but not near enough to the core of the Sc line to affect the abundance. A few weak neutral Cr, Fe, and V lines on both wings of the 5657 Å line have no influence on the abundance either.

Sc II 6245.63 Å belongs to the group of well-separated, unblended weak lines. Again, the hyperfine structure fits the observed spectra as shown in Fig. 5f. This line lies on the extended wing of Fe I (816) 6246.334 Å, but that does not change the line abundance.

Altogether, the remaining influence of blends is small, with $\Delta b = -0.021$, but it is systematic in that it always *reduces* the mean Sc abundance. It is even more important because it tends to reduce the peaks of the abundance distribution.

3.3. The solar scandium abundance

Our method of spectrum synthesis yields the product of the oscillator strength for a given transition and the abundance of the element, $\log gf\epsilon_{\odot}$. The results are reproduced in Table 1 assum-

ing NLTE conditions. Using the values obtained for $\log gf\epsilon_{\odot}$ and the $\log gf$ values from different data sets, we computed Sc abundances for the individual lines. Figure 6 shows LTE and NLTE abundance results based on the Kurucz calculated oscillator strengths for all lines as a function of their equivalent widths.

Under the LTE assumption, absolute solar abundances determined from Sc I lines are significantly lower than the values obtained for the Sc II lines. The *mean* LTE abundances for 4 Sc I and 17 Sc II lines are 2.90 ± 0.09 dex and 3.10 ± 0.05 dex, respectively. This discrepancy of the ionization equilibrium is resolved in NLTE calculations. Under NLTE assumption, Sc I and Sc II lines give very consistent abundance results, i.e. 3.08 ± 0.05 dex and 3.07 ± 0.04 dex, respectively. Using Kurucz' gf values, the mean abundance for all 21 Sc lines under NLTE is 3.07 ± 0.04 dex.

Using instead the laboratory $\log gf$ values of Lawler & Dakin, the mean abundance of 17 Sc lines under NLTE is 3.13 ± 0.05 dex. The ionization equilibrium differs by 0.03 dex. While the results for both sets of gf values are a brilliant justification of the NLTE assumption itself, it seems that the experimental gf values provided by Lawler & Dakin (1989) should be slightly more reliable than those calculated by Kurucz. However, the standard deviation of the experimental data is slightly higher.

4. Discussion

The most interesting result of this analysis turns out to be that scandium is the first element found to show strong solar NLTE *abundance* effects in one of its ions. This appears to be the consequence of missing strong lines in Sc I. All the lines of this ion are weak because of two contributions: (a) the solar scandium abundance is 3 dex lower than that of other metals, and (b) due to its low ionization energy of only 6.6 eV, Sc I is an extreme *minority ion*, that is 99.8% ionized in its solar region of line formation. Therefore it does not help that the gf values are relatively normal, and the statistical equilibrium of Sc I is far from thermal even in layers of continuum formation. The departure coefficients calculated for different values of photoionization and collision parameters (see Fig. 3) reveal the insensitivity of our results to the choice of details of the model atom. This may no longer be the case in more metal-poor stars.

Although still far from complete, the experimental *hyperfine structure* data are compatible with the observed solar line profiles, with the exception of a few lines, for which either lower or upper level HFS data are missing. We have not attempted to determine abundances without HFS, because the profile fits were far from realistic in most cases (in particular for Sc II). The general trend of such an analysis would be a relative *increase* in the abundances as a response to a decrease in line broadening, which affects mostly the few lines on the flat part of the curve-of-growth.

Depending on whether calculated gf values of Kurucz & Bell (1995) or experimental gf values of Lawler & Dakin (1989) are preferred, the solar scandium abundance is

$$\log \epsilon_{\text{Sc},\odot} = \begin{cases} 3.07 \pm 0.04 & (\text{Kurucz \& Bell}) \\ 3.13 \pm 0.05 & (\text{Lawler \& Dakin}) \end{cases} .$$

For the experimental gf values, the difference with respect to the *meteoritic* scandium abundance turns out to be as high as before. Therefore the emphasis lies on our current analysis being much more restrictive than recent results. If the higher photospheric abundance were caused by a systematic error in our analysis, this should be found in Fig. 6b. Assuming say that all

lines were affected by remaining unknown blends, the resulting abundances should show a trend with line strength (weak line abundances are more affected than strong lines). Since such a trend is not found, we may rule out the importance of unknown blends. A similar argument holds for the role of the HFS, however, now producing an inverse trend, where weak lines should not depend on the HFS.

A completely different systematic abundance error could result from the solar model atmosphere. In the above investigation we started the statistical equilibrium and the synthetic spectrum calculations with our standard ODF model atmosphere³, which is very much the same as that of Kurucz (1992), and it makes use of his opacity distribution functions, corrected for metal abundance. Such ODF models tend to have slightly lower temperatures near optical depth $\tau \simeq 1$. Opacity sampling (OS) models are different. Their higher temperatures are essentially the reason for the insufficient fit the solar Balmer lines (see Grupp 2004). Since the temperature difference for the solar OS model of Grupp is only around 40 K or less, it changes the Sc line formation by a negligible amount. The abundance entries in Table 1 document that there is a mean abundance difference in the sense ODF–OS of only -0.016 dex.

Comparison with the results obtained for the ODF model atmosphere shows that the solar scandium abundance for the laboratory gf values of Lawler & Dakin, $\log \varepsilon_{\text{Sc},\odot} = 3.13 \pm 0.05$, is off the meteoritic value of 3.04 by 0.09 dex. A large fraction of the remaining scatter of the single line abundances seen in Fig. 6b is probably caused by the uncertain gf values, both for calculated and experimental data. While previous analyses could not confirm a correspondence between photospheric and meteoritic Sc abundances due to a relatively large line-by-line scatter, our results reduce the problem to a simple discrepancy. Kurucz' f -values lead to a solar Sc abundance well in agreement with the meteoritic value, whereas the experimental data of Lawler & Dakin deviate from that reference by nearly 2σ . Currently, there is no hint as to why photospheric scandium should differ in abundance from that found in chondrites.

Acknowledgements. This project was supported by the Deutsche Forschungsgemeinschaft (DFG) under grants GE490/33-1 and 446 CHV 112/1,2/06, and by the National Natural Science Foundation of China under grants No. 10778612, 10433010, and 10521001, and by the National Key Basic Research Program (NKBRP) No. 2007CB815403. HWZ and GZ thank the Institute of Astronomy and Astrophysics of Munich University for warm hospitality during a productive stay in 2006 and 2007.

References

- Allen, C.W. 1973, *Astrophysical Quantities*, 3rd Ed., Athlone Press, London
- Anders, E., & Grevesse, N. 1989, *Geochim. Cosmochim. Acta*, 53, 197
- Anstee, S.D., & O'Mara, B.J. 1991, *MNRAS*, 253, 549
- Anstee, S.D., & O'Mara, B.J. 1995, *MNRAS*, 276, 859
- Arnesen, A., Hallin, R., Nordling, C., et al. 1982, *A&A*, 106, 327
- Asplund, M. 2005, *ARA&A*, 43, 481
- Barklem, P.S., Piskunov, N., O'Mara, B.J. 2000, *A&AS*, 142, 467
- Belyaev, A.K., Grosser, J., Hahne, J., et al. 1999, *Phys.Rev.A*, 60, 2151
- Belyaev, A.K., & Barklem, P.S. 2003, *Phys.Rev.A*, 68, 2703
- Brix F., & Kopfermann H. 1952, *Landolt-Börnstein, Zahlenwerte und Funktionen I/5*, Springer, Berlin
- Butler K., & Giddings J. 1985, *Newsletter on the analysis of astronomical spectra No. 9*, University of London
- Childs, W.J. 1971, *Phys.Rev.A*, 4, 1767
- Drawin, H.W. 1968, *Z.Physik*, 211, 404
- Drawin, H.W. 1969, *Z.Physik*, 225, 483
- Ertmer, W., & Hofer, B. 1976, *Z.Physik*, 276, 9
- Fuhrmann, K., Pfeiffer, M., Frank, C., et al. 1997, *A&A*, 323, 909

- Gehren, T., Butler, K., Mashonkina, L., et al. 2001, *A&A*, 366, 981
- Grevesse, N. 1984, *Phys.Scr.*, 8, 49
- Grevesse, N., & Noels, A. 1993, in *Origin and Evolution of the Elements*, ed. N. Prantzos, E. Vangioni-Flam, & M. Casse (Cambridge: Cambridge Univ. Press), 15
- Grevesse, N., Asplund, M., Sauval, A.J. 2007, *Space Sci. Rev.*, 130, 105
- Gratton, R.G., & Sneden, C. 1991, *A&A*, 241, 501
- Grupp, F. 2004, *A&A*, 420, 289
- Holweger, H., & Müller, E.A. 1974, *Sol. Phys.*, 39, 19
- Kurucz, R.L., Furenlid, I., Brault, J., et al. 1984, *Solar Flux Atlas from 296 to 1300nm*, Kitt Peak National Solar Observatory
- Kurucz, R.L., & Bell, B. 1995, *Atomic Line Data*, Kurucz CD-ROM No. 23., Cambridge, Mass.: Smithsonian Astrophysical Observatory
- Kurucz R.L. 1992, *Rev. Mex. Astron. Astrof.*, 23, 45
- Lawler, J.E., & Dakin, J.T. 1989, *J. Opt. Soc. Am. B*, 6, 1457
- Mansour, N.B., Dineen, T., Young, L., et al. 1989, *Phys.Rev.A*, 39, 5762
- Marsden, G.C., Den Hartog, E.A., Lawler, J.E., et al. 1988, *J. Opt. Soc. Am. B*, 5, 606
- Mihalas, D. 1978, *Stellar Atmospheres*, 2nd edition (San Francisco, W.H. Freeman & Co.), p. 99
- Neuforge, C. 1993, in *Origin and Evolution of the Elements*, ed. N. Prantzos, E. Vangioni-Flam, & M. Casse, Cambridge: Cambridge Univ. Press, 63
- Nissen, P.E., Chen, Y.Q., Schuster, W.J., et al. 2000, *A&A*, 353, 722
- Prochaska, J.X., & McWilliam, A. 2000, *ApJ*, 537, L57
- Reetz, J.K. 1991, *Diploma Thesis*, Universität München
- Seaton, M.J. 1962, in *Atomic and Molecular Processes*, Acad. Press, New York
- Seaton, M.J., Mihalas, D., Pradhan, A.K. 1994, *MNRAS*, 266, 805
- Steenbock, W., & Holweger, H. 1984, *A&A*, 130, 319
- van Regemorter H. 1962, *ApJ*, 136, 906
- Young L., Childs W.J. Dineen C. et al. 1988, *Phys.Rev.A*, 37, 4213
- Youssef, N.H., & Amer, M.A. 1989, *A&A*, 220, 281
- Zhang, H.W., Butler, K., Gehren, T., et al. 2006, *A&A*, 453, 723
- Zhao, G., & Magain, P. 1990, *A&A*, 238, 242

³ This should not lead to confusion, because the background line opacities in the statistical equilibrium calculations are *always* sampled.